Title
Recent Southern Ocean warming and freshening driven by greenhouse gas emissions and ozone depletion

Journal
Nature Geoscience, 11(11)

ISSN
1752-0894

Authors
Swart, Neil C
Gille, Sarah T
Fyfe, John C
et al.

Publication Date
2018-11-01

DOI
10.1038/s41561-018-0226-1

Peer reviewed

Recent Southern Ocean warming and freshening driven by greenhouse gas emissions and ozone depletion

Neil C. Swart[1], Sarah T. Gille[2], John C. Fyfe[1], and Nathan Gillett[1]

[1] *Canadian Centre for Climate Modelling and Analysis, Environment and Climate Change Canada, Victoria, British Columbia V8W 2Y2, Canada.*

[2] *Scripps Institution of Oceanography, University of California San Diego, La Jolla, CA, 92093-0230, USA.*

Abstract

The Southern Ocean has, on average, warmed and freshened over the past several decades. As a primary global sink for anthropogenic heat and carbon, understanding changes in the Southern Ocean is directly relevant to predicting the future evolution of the global climate system. However, the drivers of these changes are poorly understood, owing to sparse observational sampling, large amplitude internal variability, modelling uncertainties and the competing influence of multiple forcing agents. Here we construct an observational synthesis to quantify temperature and salinity changes over the Southern Ocean and combine this with an ensemble of co-sampled climate model simulations. Using a detection and attribution analysis, we show that the observed changes are inconsistent with internal variability or the response to natural forcing alone. Rather, the observed changes are primarily attributable to human

induced greenhouse gas increases, with a secondary role for stratospheric ozone depletion. Physically, the simulated changes are primarily driven by surface fluxes of heat and freshwater. The consistency between the observed changes and our simulations provides increased confidence in the ability of climate models to simulate large scale thermohaline change in the Southern Ocean.

The Southern Ocean has experienced a complex set of changes over the past several decades. There have been strong, regionally opposing trends in sea-ice since satellite observations began in 1979, with a small but significant overall increase in sea-ice cover, and an associated near-surface cooling[1;2;3]. However, below the surface, repeat observations show a significant warming trend since 1950[4;5], and a broad-scale freshening[6]. At mid-depths and within the latitudes of the Antarctic Circumpolar Current, the warming has proceeded at nearly twice the rate of global upper ocean warming[4]. The processes driving this warming make the Southern Ocean the dominant region of anthropogenic heat and carbon uptake[7;8;9]. Hence, understanding the drivers of these changes is vital for making reliable future climate projections[10;11], but is complicated by several factors.

The Southern Ocean is subject to strong internal climate variability, which may account for a substantial portion of the observed change[12;13;14;15;16]. It is also one of the more poorly sampled regions of the global ocean[5], accentuating the difficulty of quantifying forced trends. Modelling results suggest that both greenhouse gas increases[17] and stratospheric ozone depletion[18;19] are important drivers of Southern Ocean change. However, the ability of coarse resolution climate models to accurately simulate changes in the Southern Ocean, where the dynamics are modulated by small-scale eddies, has been questioned[10]. Human influence on ocean thermohaline change has previously been detected in large-scale basin averages[20;21;22;23]. However, observed patterns of Southern Ocean thermohaline change have not yet been attributed to specific forcing agents. Here we present a new observational synthesis of Southern Ocean temperature and salinity changes, address the questions of data sparsity and model skill, and then develop a framework for attributing these changes to individual forcing agents.

Observed and simulated changes

To quantify historical changes in Southern Ocean temperature and salinity, we use all hydrographic profiles available in the World Ocean Database for the period 1950-2015. We compute anomalies between each profile and the closest matching point in a modern Argo based climatology[24] to avoid aliasing due to the sparse historical sampling, and grid the data (see Methods and below).

The observed zonal-mean temperature change over the Southern Ocean, computed as the 2006-2015 mean minus the 1950-1980 mean, is dominated by a region of warming centered near 45°S and extending from the surface to over 1,500 m (Fig. 1a). An interesting exception to this warming pattern is a sub-surface cooling between about 250 and 2,000 m and between 30-36°S. Salinity shows a more complex pattern of change (Fig. 1b). The salinity pattern is dominated by a strong surface freshening south of 45°S, which extends into the ocean interior in a northward arc, which is contrasted against a strong salinification in the upper 500 m, north of 45°S. These patterns of change are largely consistent with previous observational studies[10;6].

To help understand these observed changes we turn to the Canadian Earth System Model, in which the ALL forcing experiment (including solar, volcanic, anthropogenic aerosols, ozone depletion, land use change and greenhouse gases; see Methods) was run 50 times from slightly different initial conditions to produce a large ensemble. The ensemble mean over the 50 realizations provides an estimate of the forced response - the fingerprint of change associated with the forcing, while the spread across the ensemble provides an estimate of the uncertainty due to internal climate variability. We sub-sample the model using the same coverage of historical hydrographic profiles, determined to the nearest month, to make our results directly comparable with the observations above (see Methods).

The ALL forcing fingerprints reproduce the observed patterns of change very well (Figs. 1c, d). The correlation coefficients between the simulated and observed patterns are 0.83 and 0.72 for temperature and salinity respectively. Regions where the observed changes fall within the 2.5th to 97.5th percentile spread of the 50 model realizations are indicated by stippling in Figs. 1a and b, indicating where the model and observations agree at the 5% level. Most regions are stippled, but in the non-stippled areas the model typically correctly simulates the sign of the observed change, but does not capture the correct magnitude of changes. In particular, the model underestimates the magnitude of the observed subsurface cooling and freshening, between about 30 to 42°S. This will partly be addressed by the scaling factors introduced in the detection and attribution analysis below.

The observational coverage is extremely sparse in the early part of the record and increases over time, with a step-like jump after the introduction of the Argo array in 2004 (Figs. S1, S2). We can use the model to address the question of whether the sparse observational sampling biases our estimates of temperature and salinity change since 1950, despite our careful analysis approach (see Methods). Figs. 1e and f show the patterns of change obtained when we use the full model coverage (no sub-sampling). Relative to Figs. 1c and d, in which the model was sub-sampled with observational coverage, we see minor differences in detail, but no fundamental changes in the patterns. This result suggests that the sparse observational sampling of the Southern Ocean has not systematically biased our estimates of multi-decade scale zonal mean temperature and salinity change. Analysis of more regional scales, and shorter period variability would however be increasingly subject to aliasing, and hence we do not attempt to move our analysis beyond zonal mean scales. Next we address the drivers of these observed changes.

Detection and attribution

In order to objectively compare the simulated and observed Southern Ocean changes, and to determine the relative contributions of individual climate forcings to the changes, we apply a detection and attribution analysis[25] (see Methods). We begin with a one-signal analysis, regressing observed changes (Fig. 1a, b) onto the model-derived fingerprints of change associated with ALL forcing experiment (Fig. 1c, d). The resulting scaling factors are significantly different from zero at the 5% significance level for both temperature and salinity (Fig. 2). This means that we formally detect the fingerprints of climate change in observed Southern Ocean temperature and salinity, and the observed changes are not explainable by internal climate variability alone[25]. The salinity scaling factor is consistent with unity, which means that the magnitude of the simulated changes is consistent with the observations. The temperature scaling factor of 0.74 does not include unity in its uncertainty range, implying that the model response has to be scaled down to best fit the observations. This is consistent with our knowledge that CanESM2 warms too rapidly over the historical period[26].

To identify the roles of individual forcing agents, we now conduct a multi-signal analysis (see Methods). The fingerprints are derived from four experiments, each comprising 50 simulations, in which the CanESM2 model was forced by i) greenhouse gas forcing only (GHG); ii) natural forcing only (NAT, solar and volcanic); iii) anthropogenic aerosols only (AER) and iv) stratospheric ozone depletion only (OZ). The resulting scaling factors represent the best combined fit to the observations of the fingerprints for each individual forcing (Fig. 2). The scaling factors associated with the NAT fingerprints are not significantly different from zero, indicating no detectable influence of natural forcing (solar and volcanic) in these zonal mean sections. Similarly, the AER fingerprints were not detected in the observations. By contrast we can independently detect the fingerprints of both GHG and OZ induced changes in the observed temperatures, while for salinity only the GHG fingerprint is detected. If we do a combined analysis on temperature and salinity, we can detect both the GHG and OZ patterns (Fig. S3).

The relative contribution of each forcing to the observed pattern of change (Fig. 3) is given by the fingerprints multiplied by the appropriate scaling factor. For both temperature and salinity, greenhouse gas forcing plays the dominant role (Fig. 3a, b), showing patterns of change similar to the ALL forcing experiment and observations (Fig. 1). This is consistent with the understanding that increasing greenhouse gases are the principal driver of climate warming[25] and recent anomalous ocean heat uptake[27]. In our simulations, stratospheric ozone depletion is responsible for the cooling observed north of 40°S, and for warming to the south (Fig. 3c), consistent with previous modelling studies[28;18;29]. The OZ response is distinct from the uniformly-warming GHG signal in this regard. The fact that the fingerprint of OZ forcing was detected in the observations for temperature but not salinity most likely lies in the fact that the GHG and OZ fingerprints are highly correlated for salinity (Fig. 3b, d) which makes independent detection difficult.

Based on these results, we conclude that observed Southern Ocean temperature and salinity changes are inconsistent with internal variability or natural forcing alone, but can be attributed to anthropogenic influence in general, and greenhouse gas increases and stratospheric ozone depletion in particular. These results are in agreement with the previous detection of anthropogenic influence on ocean temperature and salinity at the global scale and in other ocean basins[20;21;22;23]. We have advanced on previous work by using an updated observational synthesis to focus on the Southern Ocean patterns of change, and by attributing the observed changes to GHG and OZ forcing in particular, rather than just the combined anthropogenic signal (ALL).

Physical mechanisms

Changes in temperature and salinity on pressure surfaces (Fig. 1) can be driven by changes in surface fluxes and water masses, or by adiabatic shifts of density surfaces which do not alter water masses (known as heave), induced by wind and ocean circulation changes. To help separate these effects, we recompute the changes on isopycnal surfaces $26 \leq \sigma_\theta \leq 27.75$, comprising the main watermasses of the Antarctic Circumpolar Current (Fig. 4). The observations show a warming and salinification of Upper Circumpolar Deep Water centered on $\sigma_\theta = 27.5$, south of 45°S, and a cooling and freshening of thermocline waters north of this and centered on $\sigma_\theta = 27.0$ (Figs. 4a, b). The CanESM2 ALL forcing simulation overall shows similar patterns of change (Figs. 4c, d), though the model does have some climatological biases in water mass structure, and the cooling/freshening tends to occur in lighter density classes than observed. Overall, these patterns of change are consistent with previously identified water mass changes in the Southern Ocean[30;31;32;10], and imply water mass modification by surface fluxes.

In the model, a heat budget analysis of the ALL forcing experiment shows that 75% of depth-integrated warming in the Southern Ocean can be explained by overlying anomalous surface heat fluxes (Figs. 5a, c). Given conservation of heat, we can infer that the remaining 25% of the simulated warming is driven by anomalous ocean heat transport across the boundaries of the domain. The salinity budget shows that most of the additional freshwater enters the ocean to the south of the boundary of our analysis area at 60°S (Figs. 5b, d), and then is advected into the analysis region by the prevailing northward Ekman transport. These results are consistent with a previous study[1], which argues that Southern Ocean warming is largely driven by anomalous surface fluxes combined with the climatological transport, and that changes in transport play only a secondary role. In our simulations the Southern Ocean Meridional Overturning Circulation (MOC) does change (Fig. S4), mostly driven by GHG forcing, and intensified westerly winds (Fig. S5), while the Antarctic Circumpolar Current shows only a very small increase in strength (Fig. S6).

Previous studies proposed that observed Southern Ocean warming may be associated with poleward shifts of the Southern Ocean fronts[5;10]. The additional constraint of salinity changes suggests that this is unlikely the case. Since salinity increases towards the north over the upper water column, the observed pattern of freshening is inconsistent with a simple southward shift of isopycnals (i.e. fronts). Indeed, recent studies find no evidence that the Southern Ocean fronts have shifted poleward[33;34]. It is also interesting to note that CanESM2 does not include an interactive ice sheet, but is able to simulate the observed large scale salinity change in the Southern Ocean north of 60°S. This is evidence that the observed salinity changes are not primarily driven by freshwater input from ice sheet melt, which is small relative to changes in precipitation minus evaporation[35;36;6] and northward advection of freshwater by sea-ice[37;38].

Implications for the future

Our detection and attribution analysis shows that the thermohaline changes simulated by CanESM2 are statistically consistent with the observed changes. This provides increased confidence in the ability of coarse resolution climate models ($\approx 1^\circ$) to simulate large scale temperature and salinity changes in the Southern Ocean. Our attribution results also indicate that greenhouse gas forcing dominated over ozone depletion in the observed warming and freshening of Southern Ocean since 1950 (Fig. 3). Given this, we expect to see continued warming and freshening of the Southern Ocean over the coming decades, despite the mitigating effects of ozone recovery[39;40]. Such changes are highly relevant for the future of Southern Ocean sea-ice[29;12], the Antarctic ice-sheets[41], and the global ocean uptake of heat and carbon[7;8;9].

Methods

Observations

Since the observational record is sparse, particularly in the early part of the record (Fig. S1), we need to compute anomalies carefully to avoid aliasing. For a reliable baseline, we use the well sampled modern Argo era (2004-2008), and specifically the gridded Roemmich and Gilson (RG) Argo based climatology[24], which is available at `http://sio-argo.ucsd.edu/RG_Climatology.html`. For every historical profile available in the World Ocean Database (`https://www.nodc.noaa.gov/OC5/WOD/pr_wod.html`) for the period 1950-2015, we compute the temperature and salinity anomaly relative to the RG climatological value for the same month, and the closest position in space to the profile. Computing anomalies in such a manner is used to avoid seasonal and spatial aliasing effects resulting from averaging sparse observations[10]. We then bin-average these observed anomalies in space onto the CanESM2 model grid, with a nominal resolution of 1° in latitude and 1.5° in longitude and at a time resolution of one month. After using this monthly resolved data to define the sub-sampling of the model (see below), we further average to 5-year means. Finally we compute the differences between the mean over the decade 2006 to 2015 minus the base period, which is a mean over 1950 to 1980.

CanESM2 large ensembles

We use the Canadian Earth System Model version 2[42;43], the version of the model used for the Coupled Model Intercomparison Project Phase 5. The model consists of the CanAM4 atmosphere model, run at T63 spectral resolution and coupled to the CanOM4 ocean model, which has a nominal resolution of 1° in latitude and 1.5° in longitude. CanESM2 includes a land surface scheme (CLASS) and interactive carbon cycle components on the land (CTEM) and in the Ocean (CMOC).

Four CMIP5 attribution experiments were conducted with the model: i. all forcing (ALL); ii. natural forcing only (NAT, solar and volcanic); iii. anthropogenic aerosols only (AER) and iv. stratospheric ozone depletion only (OZ). In all cases the model was run over the historical period (1950-2005), and this was joined with future runs using the appropriate forcing from the Representative Concentration Pathway 8.5 (2006-2100). We are only interested in the period extending from 1950 to 2015. There is very little difference between the RCPs between 2006 and 2015. For each experiment, the initial condition in 1950 is taken from the 5 CanESM5 realizations submitted to the CMIP5 archive. In this year, the five realizations were branched into 50 realizations per experiment (for a total of 200), by introducing a random permutation to the seed used in the random number generator for cloud physics, and then integrated forwards under the appropriate historical/RCP8.5 forcing. No other perturbation is made to the realizations, but the subtle change to the random seed for cloud physics ensures that internal variability diverges rapidly across the realizations. Therefore, within each experiment, the forcing is identical, and the runs only differ in their realization of internal variability.

A large ensemble was not run with greenhouse gas (GHG) forcing only, but we are interested in the the impacts of GHGs alone. The difference between the all forcing experiment and the sum of the other three provides an estimate of the influence of greenhouse gases, under the assumption that the responses to these forcings sum linearly (i.e. ALL = GHG + NAT + OZ + AER). We can verify that this assumption holds by comparing to five CanESM2 simulations forced by GHG only, which were submitted to CMIP5. The ensemble mean response to GHG forcing inferred from the large ensembles, using the assumption of linearity above, is nearly identical to the ensemble mean response in the five actual GHG-only simulations (Fig. S7).

In the model at each spatial point and for each month, we compute anomalies relative to the model climatology over 2004 to 2008 (the same period used to compute the RG observed climatology - the model and RG baseline climatologies both have complete spatial coverage).

The observations have many grid points that contain no data. We use the missing data-mask from the observations, and apply it to the model, so that data coverage is exactly consistent between them. After this point, all averages are applied in the same way to the model and observations, ensuring consistent sampling. Specifically, we bin-average the data into 5-year means, then we compute differences between the mean over the decade 2006 to 2015 minus the base period, which is a mean over 1950 to 1980.

While the large size of the CanESM2 ensemble provides robust estimates of the forced response (fingerprints), and the range of internal variability, it does not sample model uncertainty. However, the warming pattern in CanESM2 is consistent with the average across the CMIP5 models[1].

Detection and attribution methodology

In the context of our study, detection means demonstrating that the Southern Ocean temperature and salinity have changed in a statistical sense, and that this change is inconsistent with internal variability. Attribution means determining the relative contributions of multiple climate forcings to the change, with an assigned statistical confidence[25]. Attribution to a specific forcing is done by showing that the observed changes are consistent with the process-based model (CanESM2) which includes the forcing (e.g. greenhouse gas increases), but is inconsistent with an otherwise identical model that excludes this forcing.

We adopt the widely used fingerprinting approach, which means that we assume that the model simulates the pattern (or fingerprint) of the response to external forcing, but not necessarily the correct magnitude of the response[25]. For each of the four experiments (GHG, NAT, AER, OZ, see main text), the fingerprint is the ensemble mean over 50 model realizations, which differ only in their rendition of internal variability. The analysis produces scaling factors, which describe how the magnitude of the model response to individual forcings should be scaled up or down to best match the observations, and associated uncertainty estimates[25].

To obtain the scaling factors, we regress the observed changes onto the simulated fingerprint(s). In the one signal case the observations are regressed on the ALL forcing fingerprint. In the multi-signal case, a multiple linear regression is used to regress the observations onto the fingerprints for each of the four experiments. Since the simulated forced response is estimated from the ensemble mean of a 50-member ensemble, internal variability in the forced response is negligible, and we use an ordinary least squares regression[25].

To estimate uncertainty of the coefficients, we compute the residual between each realization and the ensemble mean from its experiment, which provides us with 200 realizations of internal variability. We rescale the realization by $\sqrt{50/49}$ to account for subtraction of the ensemble mean[44]. We then repeat the regressions 200 times, in each iteration replacing the observations with a different realization of the variability. That is we regress the realization of internal variability against the ensemble means. The spread (5th to 95th percentile) in parameters derived in this way provides the uncertainty in the scaling factors, and informs us of the likelihood of obtaining the scaling factors due to internal variability alone. This confidence interval allows us to evaluate if the scaling factors are significantly different from zero at the 5% level. For display purposes we center this distribution of scaling factors on the corresponding regression coefficient of the forced response in Fig. 2. Our approach leverages the large number of independent samples of internal variability available to avoid the need to estimate uncertainty intervals from an ill-conditioned covariance matrix and to avoid assuming normally distributed internal variability, as has been done previously[22].

Using different variables that are physically linked, such as temperature and salinity, can increase signal detectability[23]. For the combined temperature and salinity analysis (Fig. S3), the temperature and salinity fingerprints used above were normalized (i.e. the mean was removed, and they were divided by the standard deviation). The data were then concatenated (producing a series double the length of the temperature or salinity data alone), and the above analysis was repeated.

Code availability

Analysis code is available from the authors upon request.

Data Availability

All data used in this manuscript are publicly available. The CanESM2 large ensembles are available at `http://open.canada.ca/data/en/dataset/aa7b6823-fd1e-49ff-a6fb-68076a4a477c`. The Roemmich and Gilson Argo climatology is available at `http://sio-argo.ucsd.edu/RG_Climatology.html`. The historical profiles from the World Ocean Database can be found at `https://www.nodc.noaa.gov/OC5/WOD/pr_wod.html`.

References

[1] Armour, K., Marshall, J., Scott, J., Donohoe, A. & Newsom, E. Southern Ocean warming delayed by circumpolar upwelling and equatorward transport. *Nature Geosci* **9**, 549–554 (2016).

[2] Fan, T., Deser, C. & Schneider, D. P. Recent Antarctic sea ice trends in the context of Southern Ocean surface climate variations since 1950. *Geophys Res Lett* **41**, 2419–2426 (2014).

[3] Parkinson, C. L. & Cavalieri, D. J. Antarctic sea ice variability and trends, 1979-2010. *The Cryosphere* **6**, 871–880 (2012).

[4] Gille, S. T. Warming of the Southern Ocean Since the 1950s. *Science* **295**, 1275–1277 (2002).

[5] Gille, S. T. Decadal-Scale Temperature Trends in the Southern Hemisphere Ocean. *J. Climate* **21**, 4749–4765 (2008).

[6] Durack, P. J. & Wijffels, S. E. Fifty-year yrends in global ocean salinities and their relationship to broad-scale warming. *J Climate* **23**, 4342–4362 (2010).

[7] Roemmich, D. *et al.* Unabated planetary warming and its ocean structure since 2006. *Nature Clim. Change* **5**, 240–245 (2015).

[8] Khatiwala, S., Primeau, F. & Hall, T. Reconstruction of the history of anthropogenic CO2 concentrations in the ocean. *Nature* **462**, 346–349 (2009).

[9] Frölicher, T. L. *et al.* Dominance of the Southern Ocean in Anthropogenic Carbon and Heat Uptake in CMIP5 Models. *J Climate* **28**, 862–886 (2015).

[10] Böning, C., Dispert, A., Visbeck, M., Rintoul, S. & Schwarzkopf, F. The response of the Antarctic Circumpolar Current to recent climate change. *Nature Geosci* **1**, 864–869 (2008).

[11] Gent, P. R. & Danabasoglu, G. Response to Increasing Southern Hemisphere Winds in CCSM4. *J Climate* **24**, 4992–4998 (2011).

[12] Swart, N.C. & Fyfe, J.C. The influence of recent Antarctic ice sheet retreat on simulated sea ice area trends. *Geophysical Research Letters* **40**, 4328–4332.

[13] Polvani, L. M. & Smith, K. L. Can natural variability explain observed Antarctic sea ice trends? New modeling evidence from CMIP5. *Geophys Res Lett* **40**, 3195–3199 (2013).

[14] Gagné, M.-È., Gillett, N. P. & Fyfe, J. C. Observed and simulated changes in Antarctic sea ice extent over the past 50 years. *Geophys Res Lett* **42**, 90–95 (2015).

[15] Zunz, V., Goosse, H. & Massonnet, F. How does internal variability influence the ability of CMIP5 models to reproduce the recent trend in Southern Ocean sea ice extent? *The Cryosphere* **7**, 451–468 (2013).

[16] Lovenduski, N. S., Fay, A. R. & McKinley, G. A. Observing multidecadal trends in Southern Ocean CO2 uptake: What can we learn from an ocean model? *Global Biogeochemical Cycles* **29**, 416–426 (2015).

[17] Fyfe, J. Southern Ocean warming due to human influence. *Geophysical Research Letters* **33**, L19701 (2015).

[18] Sigmond, M., Reader, M. C., Fyfe, J. C. & Gillett, N. P. Drivers of past and future Southern Ocean change: Stratospheric ozone versus greenhouse gas impacts. *Geophys Res Lett* **38**, L12601 (2011).

[19] Solomon, A., Polvani, L. M., Smith, K. L. & Abernathey, R. P. The impact of ozone depleting substances on the circulation, temperature, and salinity of the Southern Ocean: An attribution study with CESM1(WACCM). *Geophys Res Lett* **42**, 5547–5555 (2015).

[20] Barnett, T. P., Pierce, D. W. & Schnur, R. Detection of Anthropogenic Climate Change in the World's Oceans. *Science* **292**, 270–274 (2001).

[21] Barnett, T. P. *et al.* Penetration of Human-Induced Warming into the World's Oceans. *Science* **309**, 284–287 (2005).

[22] Pierce, D. *et al.* Anthropogenic Warming of the Oceans: Observations and Model Results. *Journal of Climate* **19**, 1873–1900 (2006).

[23] Pierce, D. W., Gleckler, P. J., Barnett, T. P., Santer, B. D. & Durack, P. J. The fingerprint of human-induced changes in the ocean's salinity and temperature fields. *Geophys Res Lett* **39**, L21704 (2012).

[24] Roemmich, D. & Gilson, J. The 2004–2008 mean and annual cycle of temperature, salinity, and steric height in the global ocean from the Argo Program. *Prog Oceanogr* **82**, 81–100 (2009).

[25] Bindoff, N. *et al.* Detection and Attribution of Climate Change: from Global to Regional. In Stocker, T. *et al.* (eds.) *Climate Change 2013: The Physical Science Basis. Contribution of Working Group I to the Fifth Assessment Report of the Intergovernmental Panel on Climate Change* (Cambridge University Press, 2013).

[26] Gillett, N. P., Arora, V. K., Matthews, D. & Allen, M. R. Constraining the Ratio of Global Warming to Cumulative CO2 Emissions Using CMIP5 Simulations. *J Climate* **26**, 6844–6858 (2013).

[27] Levitus, S. *et al.* Anthropogenic Warming of Earth's Climate System. *Science* **292**, 267–270 (2001).

[28] Bitz, C. & Polvani, L. Antarctic climate response to stratospheric ozone depletion in a fine resolution ocean climate model. *Geophys Res Lett* **39**, L20705 (2012).

[29] Sigmond, M. & Fyfe, J. C. Has the ozone hole contributed to increased Antarctic sea ice extent? *Geophys Res Lett* **37**, L18502 (2010).

[30] Bindoff, N. L. & McDougall, T. J. Decadal changes along an Indian Ocean section at 32°S and their interpretation. *J Phys Oceanogr* **30**, 1207–1222 (2000).

[31] Banks, H. T. & Bindoff, N. L. Comparison of Observed Temperature and Salinity Changes in the Indo-Pacific with Results from the Coupled Climate Model HadCM3: Processes and Mechanisms. *J Climate* **16**, 156–166 (2003).

[32] Aoki, S., Bindoff, N. & Church, J. Interdecadal water mass changes in the Southern Ocean between 30°E and 160°E. *Geophys Res Lett* **32**, L07607 (2005).

[33] Gille, S. T. Meridional displacement of the Antarctic Circumpolar Current. *Philosophical Transactions of the Royal Society of London A: Mathematical, Physical and Engineering Sciences* **372** (2014).

[34] Freeman, N. M., Lovenduski, N. S. & Gent, P. R. Temporal variability in the Antarctic Polar Front (2002-2014). *J Geophys Res Oceans* **121**, 7263–7276 (2016).

[35] Pauling, A. G., Bitz, C. M., Smith, I. J. & Langhorne, P. J. The Response of the Southern Ocean and Antarctic Sea Ice to Freshwater from Ice Shelves in an Earth System Model. *J Climate* **29**, 1655–1672 (2016).

[36] Fyfe, J. C., Gillett, N. P. & Marshall, G. J. Human influence on extratropical Southern Hemisphere summer precipitation. *Geophys Res Lett* **39**, L23711 (2012).

[37] Abernathey, R. *et al.* Water-mass transformation by sea ice in the upper branch of the Southern Ocean overturning. *Nature Geosci* **9**, 596 (2016).

[38] Haumann, A., Gruber, N., Münnich, M., Frenger, I. & Kern, S. Sea-ice transport driving Southern Ocean salinity and its recent trends. *Nature* **537**, 89–92 (2016).

[39] Polvani, L. M., Previdi, M. & Deser, C. Large cancellation, due to ozone recovery, of future Southern Hemisphere atmospheric circulation trends. *Geophysical Research Letters* **38**, L04707 (2011).

[40] Previdi, M. & Polvani, L. M. Climate system response to stratospheric ozone depletion and recovery. *Quarterly Journal of the Royal Meteorological Society* **140**, 2401–2419 (2014).

[41] Pritchard, H. D. *et al.* Antarctic ice-sheet loss driven by basal melting of ice shelves. *Nature* **484**, 502–505 (2012).

[42] Arora, V. K. *et al.* Carbon emission limits required to satisfy future representative concentration pathways of greenhouse gases. *Geophys Res Lett* **38**, L05805 (2011).

[43] Yang, D. & Saenko, O. A. Ocean Heat Transport and Its Projected Change in CanESM2. *J Climate* **25**, 8148–8163 (2012).

[44] Stone, D., Allen, M. R., Selten, F., Kliphuis, M. & Stott, P. A. The Detection and Attribution of Climate Change Using an Ensemble of Opportunity. *J Climate* **20**, 504–516 (2007).

Acknowledgements

We acknowledge Environment and Climate Change Canada's Canadian Centre for Climate Modelling and Analysis for executing and making available the CanESM2 Large Ensemble simulations used in this study, and the Canadian Sea Ice and Snow Evolution Network for proposing the simulations. STG acknowledges NSF awards PLR-1425989 and OCE 1658001.

Author contributions

NCS conducted the analysis the wrote the paper. STG obtained and pre-processed the observational data. JCF proposed the paper. NG advised on detection and attribution. All authors contributed scientific interpretation of the results, and helped to edit the paper.

Additional Information

Supplementary information is attached. Correspondence and requests for materials should be addressed to N.C.S. (email: neil.swart@canada.ca).

Competing financial interests

The authors declare that they have no competing financial interests.

Figure 1: **Observed and simulated changes in temperature and salinity.** Zonal mean temperature (a, c, e) and salinity changes (b, d, e) from observations (a, b), the ensemble mean of CanESM2 ALL forcing experiment, sub-sampled to match the observational coverage (c, d), and the ensemble mean of CanESM2 ALL forcing ensemble with full sampling (e, f). The stippling in a and b show where the observations fall within the 2.5th to 97.5th percentile spread across the model ensemble. The anomalies represent the difference between the 2006-2015 mean and the mean over a 1950-1980 base period. Black contours are the climatological temperatures and salinities.

Figure 2: **Detection and attribution scaling factors**. a) Temperature and b) salinity scaling factors are shown for a one-signal analysis of the ALL forcing experiment, and for the multi-signal analysis using the greenhouse gas only (GHG), stratospheric ozone depletion only (OZ), natural forcing only (NAT) and anthropogenic aerosol only (AER) experiments. Scaling factors are the regression coefficients between the observations and the ensemble mean patterns of change for each experiment. The 90% confidence intervals (grey bars) were generated from the spread across the 200 individual realizations of model internal variability (see Methods), with the individual ensemble members shown as small black dots.

Figure 3: **Fingerprints of temperature and salinity change**. Zonal mean temperature (a, c) and salinity changes (b, d) from the ensemble means of CanESM2 single forcing experiments using greenhouse gas only (GHG) and stratospheric ozone depletion only (OZ) forcing. All are sub-sampled to match the observational coverage. The anomalies represent the difference between the 2006-2015 mean and the mean over a 1950-1980 base period. Note, fields have been scaled to best match observations using the scaling factors from Fig. 2.

Figure 4: **Observed and simulated changes in temperature and salinity in density space.** As in Fig. 1, but with anomalies computed in density space. Zonal mean temperature (a, c, e) and salinity changes (b, d, e) from observations (a, b), the ensemble mean of CanESM2 ALL forcing experiment, sub-sampled to match the observational coverage (c, d), and the ensemble mean of CanESM2 ALL forcing ensemble with full sampling (e, f). The anomalies represent the difference between the 2006-2015 mean and the mean over a 1950-1980 base period. Black contours are the climatological temperatures and salinities. σ_θ is potential density, referenced to the surface, minus 1000 kg m^{-3}.

Figure 5: **Southern Ocean heat and salt budget**. Change in simulated Southern Ocean volume integrated (30-60°S, 0-2000 m) heat (a) and salt (b) content, along with cumulative changes in the area-integrated surface heat and (virtual) salt fluxes. Changes in zonal mean surface heat (c) and salt (d) fluxes in time over 10-80°S. In a) contributions from shortwave radiation (SW), longwave radiation (LW) and latent (LA) and sensible (SE) heat and the flux below sea-ice (ICE) are shown. In b) E-P is evaporation minus precipitation. Dashed lines in c) and d) show latitudes 30° and 60°S. Results are for the CanESM2 ALL forcing experiment.

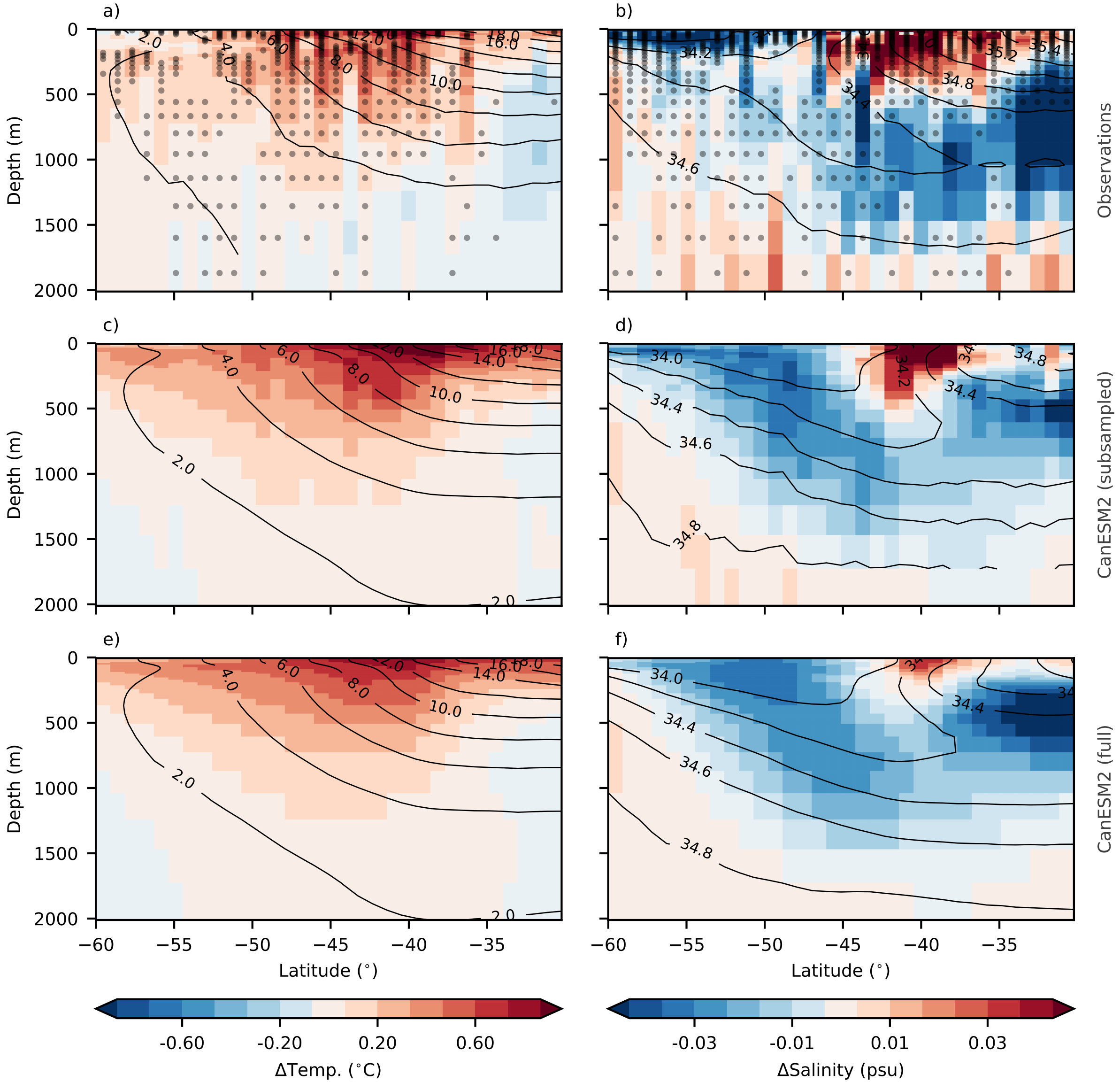

a)
b)
c)
d)
e)
f)
Depth (m)
Observations
CanESM2 (subsampled)
CanESM2 (full)
Latitude (°)
ΔTemp. (°C)
ΔSalinity (psu)
-0.60
-0.20
0.20
0.60
-0.03
-0.01
0.01
0.03

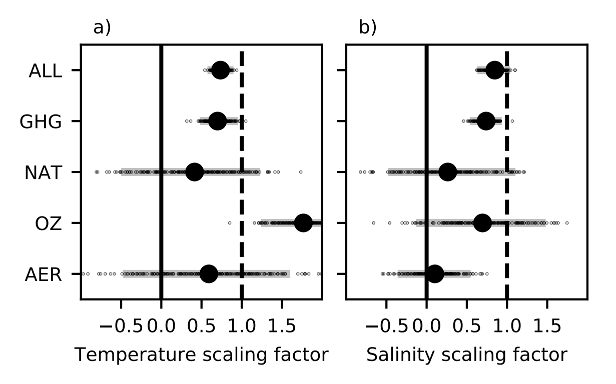

a)
b)
ALL
GHG
NAT
OZ
AER
−0.5
0.0
0.5
1.0
1.5
Temperature scaling factor
Salinity scaling factor

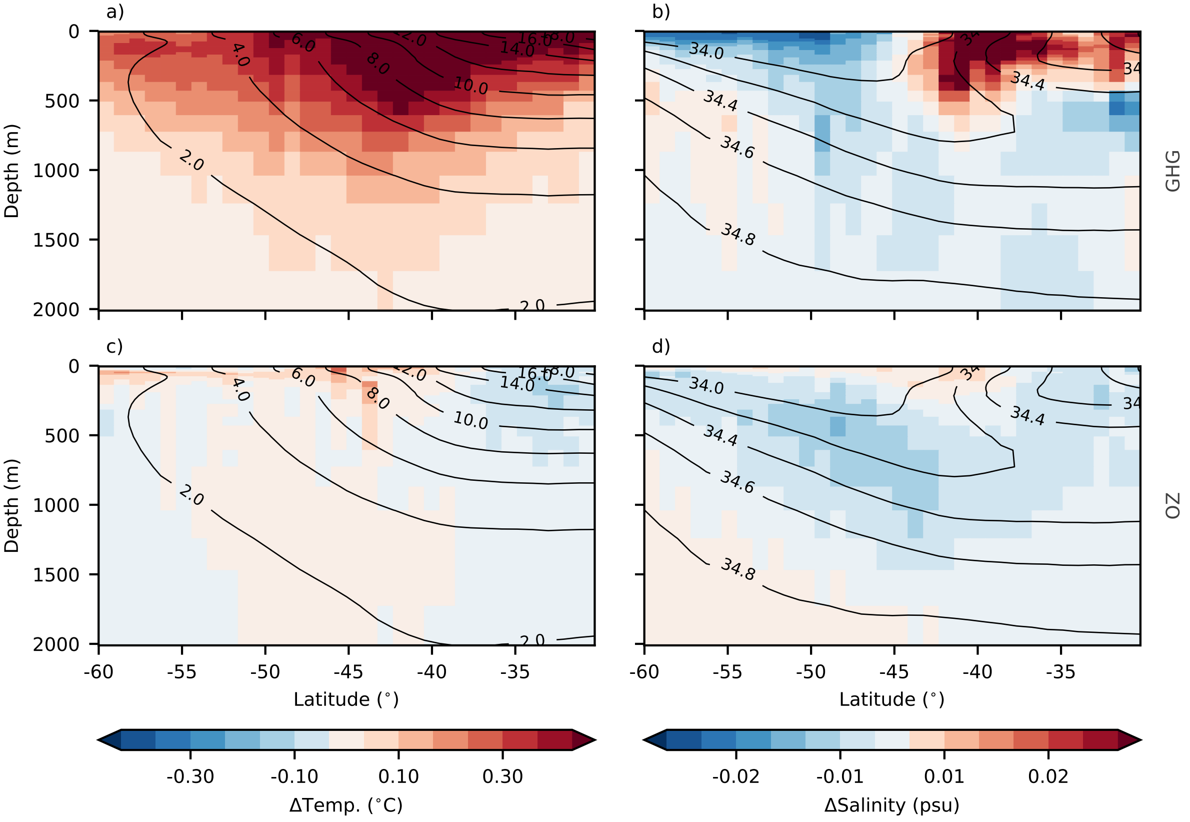

a)
b)
c)
d)
Depth (m)
Latitude (°)
GHG
OZ
ΔTemp. (°C)
ΔSalinity (psu)
-0.30
-0.10
0.10
0.30
-0.02
-0.01
0.01
0.02

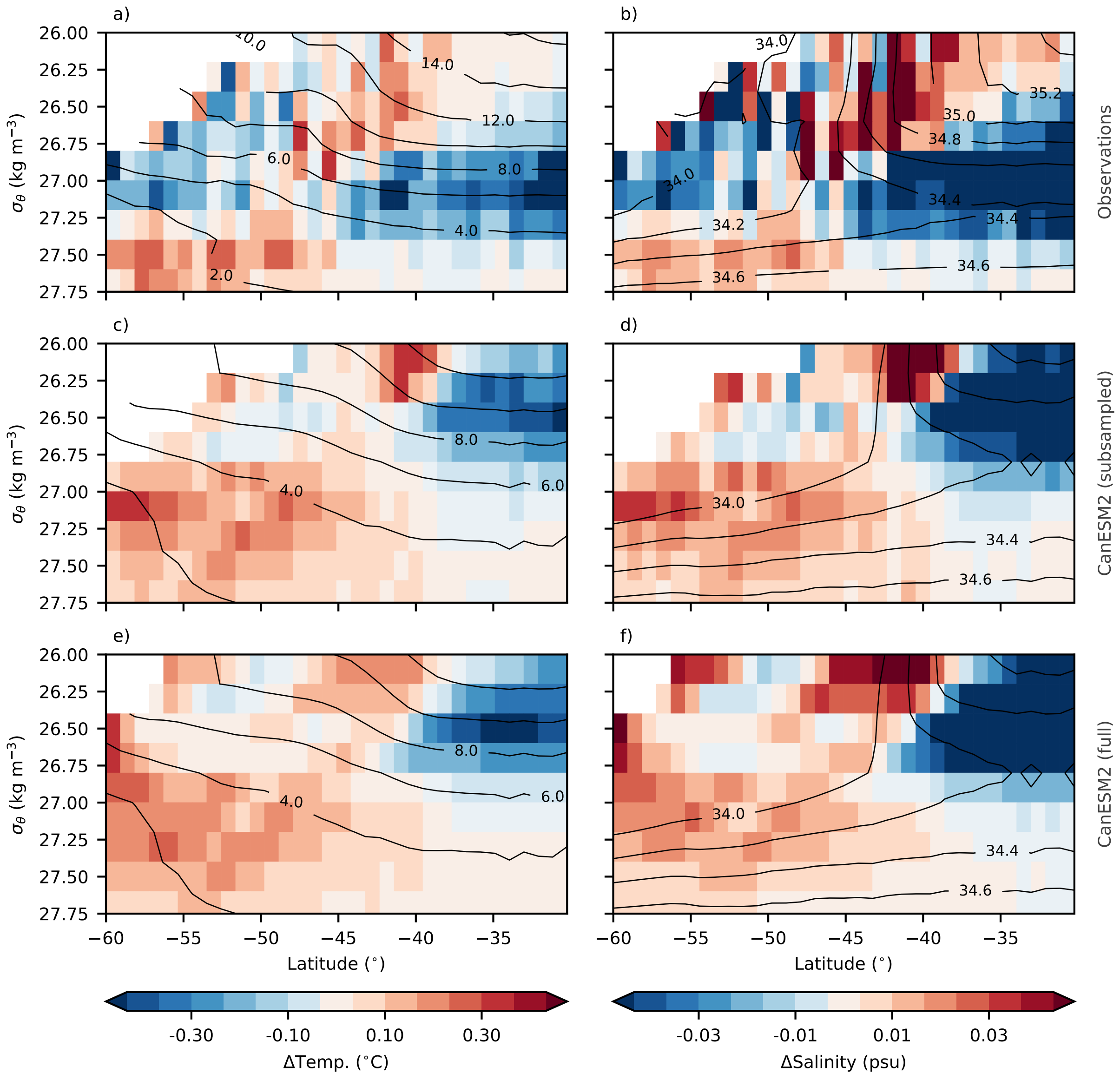

a)
b)
c)
d)
e)
f)
Observations
CanESM2 (subsampled)
CanESM2 (full)
σ_θ (kg m^{-3})
Latitude (°)
ΔTemp. (°C)
ΔSalinity (psu)
-0.30
-0.10
0.10
0.30
-0.03
-0.01
0.01
0.03

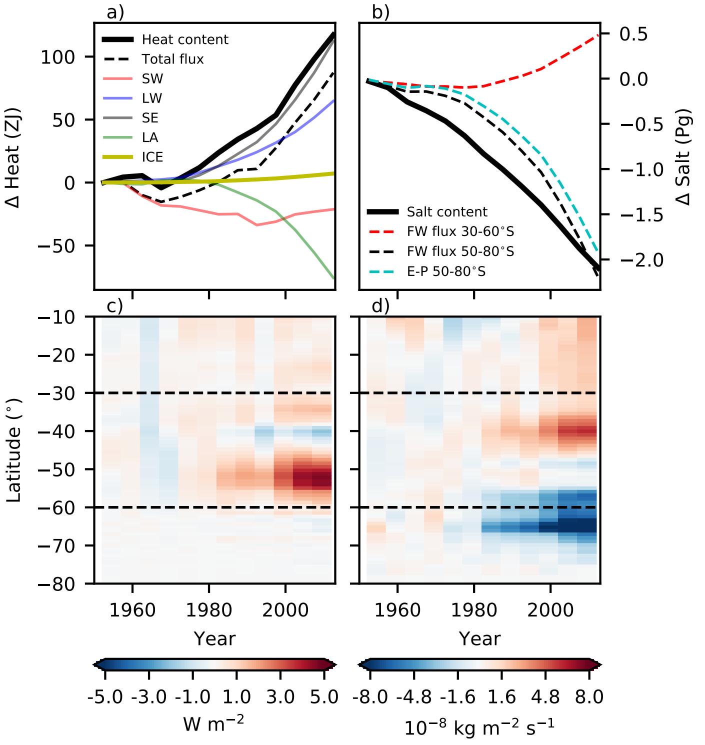

a)
Heat content
Total flux
SW
LW
SE
LA
ICE
Δ Heat (ZJ)
100
50
0
−50
b)
Salt content
FW flux 30-60°S
FW flux 50-80°S
E-P 50-80°S
Δ Salt (Pg)
0.5
0.0
−0.5
−1.0
−1.5
−2.0
c)
d)
Latitude (°)
−10
−20
−30
−40
−50
−60
−70
−80
1960
1980
2000
Year
-5.0 -3.0 -1.0 1.0 3.0 5.0
W m^{-2}
-8.0 -4.8 -1.6 1.6 4.8 8.0
10^{-8} kg m^{-2} s^{-1}